

# Noisy Qudit vs Multiple Qubits : Conditions on Gate Efficiency

Denis Janković,<sup>1, 2,\*</sup> Jean-Gabriel Hartmann,<sup>1, †</sup> Mario Ruben,<sup>2, 3, 4, ‡</sup> and Paul-Antoine Hervieux<sup>1, §</sup>

<sup>1</sup>*Université de Strasbourg, CNRS, Institut de Physique et Chimie des Matériaux de Strasbourg, UMR 7504, 23, Rue du Loess, 67000 Strasbourg, France*

<sup>2</sup>*Institute of Nanotechnology, Karlsruhe Institute of Technology, P.O. Box 3640, 76021 Karlsruhe, Germany*

<sup>3</sup>*Institute for Quantum Materials and Technologies (IQMT), Karlsruhe Institute of Technology, P.O. Box 3640, 76021 Karlsruhe, Germany*

<sup>4</sup>*Centre Européen de Science Quantique (CESQ), Institut de Science et d'Ingénierie Supramoléculaires (ISIS), Université de Strasbourg, 8, Allée Gaspard Monge, 67000 Strasbourg, France*

(Dated: February 10, 2023)

Today, multiple new platforms are implementing *qudits*,  $d$ -level quantum bases of information, for Quantum Information Processing (QIP). It is, therefore, crucial to study their efficiencies for QIP compared to more traditional qubit platforms. We present a comparative study of the infidelity scalings of a qudit and  $n$ -qubit systems, both with identical Hilbert space dimensions and noisy environments. The first-order response of the Average Gate Infidelity (AGI) to the noise in the Lindblad formalism, which was found to be gate-independent, was calculated analytically in the two systems being compared. This yielded a critical curve  $O(d^2/\log_2(d))$  of the ratio of their respective gate times in units of decoherence time. This quantity indicates how time-efficient operations on these systems are. The curve delineates regions where each system has a higher rate of increase of the AGI than the other. This condition on gate efficiency was applied to different existing platforms. It was found that specific qudit platforms possess gate efficiencies competitive with state-of-the-art qubit platforms. Numerical simulations complemented this work and allowed for discussion of the applicability and limits of the linear response formalism.

## I. INTRODUCTION

The paradigmatic bases of information in Quantum Information Processing (QIP) are qubits: two-level individually addressable quantum systems. However, several QIP platforms have recently been proposed that instead make use of  $d$ -level systems, referred to as qudits [1–3]. In its infancy, classical computing did experiment with ternary, quaternary, or higher-dimensional, bases of information, before eventually settling on the simplest (bits), when near-zero error rates and easy scalability were attained [4]. Analogously, it could be argued that quantum computing is likely to follow a similar trend in the long-term; as fault-tolerant platforms emerge and technologies mature, the industry could indeed fully settle on multiqubit systems. However, QIP research is currently not in the noise-free regime but near it, and in order to reach significant quantum supremacy [5], increasing the total Hilbert space dimension of the physical platform is a primordial requirement. As such, there is a current race to increase the number  $n$  of coupled qubits ( $d = 2$ ) with superconducting platforms leading the way with  $n = 51$  [6] or  $n = 433$  [7]. While in general the Hilbert space dimension increases exponentially in the number of sites, the relatively slow  $2^n$  scaling of qubits, compared to  $d^n$  for qudits, is proving challenging, neces-

sitating ever-more robust systems and complex control mechanisms.

Given these current technical challenges, most qudit-based platforms that have been physically implemented argue for near-term advantages over equivalent multi-qubit implementations. Thus, the principal motivations of qudit platforms over qubits include: (i) the underlying physical systems having lower decoherence rates [8], (ii) using the redundancy in additional levels for quantum error correction [9, 10], (iii) the higher density of information per physical system (site) [11] or (iv) more robust flying quantum memories [12, 13]. Furthermore, qudits present fundamental theoretical advantages, enabling novel QIP capabilities offered by  $\bigotimes SU(d)$  vs.  $\bigotimes SU(2)$  of qubits [14], and therefore a fault-tolerant qudit quantum computer indeed remains conceivable. Hence, qudits provide an alternative scaling solution by linearly increasing  $d$ , as well as increasing efficiency through single qudit gates operating on larger computational subspaces [3, 6, 15, 16]. However, one of the disadvantages raised for qudits is the larger number of error channels compared to multiple qubits [17]. In this context, a study of the near-term viability of qudits is needed to investigate the interplay between computational efficiency and noise error rates in higher dimensions.

In this work we study the Average Gate Infidelities (AGI) of single qudit and multiqubit systems, in the context of near noise-free implementations. Comparing systems of equivalent Hilbert space dimension undergoing arbitrary unitary transformations, we investigate the respective growth rates of the AGIs with respect error rates  $\gamma$  and dimensionless gate time  $\gamma t$ .

\* [jankovic@ipcms.unistra.fr](mailto:jankovic@ipcms.unistra.fr)

† [jean-gabriel.hartmann@ipcms.unistra.fr](mailto:jean-gabriel.hartmann@ipcms.unistra.fr)

‡ [mario.ruben@kit.edu](mailto:mario.ruben@kit.edu)

§ [hervieux@unistra.fr](mailto:hervieux@unistra.fr)

In sec.II a gate-independent formula is presented for the first-order response in  $\gamma t$  of the AGI to Markovian noise in the Lindblad formalism. The first-order formalism corresponds to the quasi-errorless regime of near-term QIP systems. Expressions for the linear dependency of the AGI in  $\gamma t$  for a single qudit, multiqubits and also multiqudits are derived for an arbitrary collapse operator. A comparison is then made between the rate of increase of the AGI of a single qudit vs. equivalent multiple qubits.

In sec.III numerical simulations, performed with the PYTHON package QUTiP [18], complement and illustrate the analytical results. Discussions of the applicability and limits of the linear response formalism for AGI are given and the following aspects are studied: (i) the applicable range of  $\gamma t$  and its dependency on the dimension of the qudit; (ii) the extent of the gate-independence of the result; (iii) the applicability to noise models other than pure dephasing; and finally (iv) the conditions on gate times for which either qudits or multiple qubits are advantageous. This latter aspect is then examined in more detail with respect to existing platforms.

## II. INFIDELITY INDUCED BY A PERTURBATIVE NON-UNITARY NOISE

### A. Fluctuation-dissipation relation

Consider a qudit, a  $d$ -level quantum system whose dynamics are governed by the Lindblad master equation [19]:

$$\frac{d\rho}{dt} = -i[H, \rho] + \sum_{k=1}^K \gamma_k \left( L_k \rho L_k^\dagger - \frac{1}{2} \{ L_k^\dagger L_k, \rho \} \right), \quad (1)$$

where  $\rho(t)$  is the density matrix of the system at time  $t$ ,  $H$  the Hamiltonian of the system,  $L_k$  the so-called *collapse operators* characterizing the Markovian noise, and  $\gamma_k$  the decay parameters for each of the  $K$  noise processes.

The aim is to study the effect of a single collapse operator  $\sqrt{\gamma_1} L_1 = \sqrt{\gamma} L$  on short timescales and under small-amplitude noise, i.e.,  $\gamma t \ll 1$ . Under these assumptions, one can consider an *ansatz* of the form [20]

$$\rho(t) = \rho^* - \gamma t M + o(\gamma t), \quad (2)$$

with  $\rho^*$  the noiseless target state, which is the solution of  $\dot{\rho} = -i[H, \rho]$  after time  $t$ , and  $M$  the perturbation matrix resulting from the presence of a small-amplitude noise.

One can easily see that the use of (2) in (1) leads to

$$M = \frac{1}{2} \{ L^\dagger L, \rho^* \} - L \rho^* L^\dagger. \quad (3)$$

Consider now a quantum operation bringing the initial state  $\rho_0$  to a final state  $\rho(t)$  at time  $t$ . One defines the *fidelity*  $\mathcal{F}$  of this final state relative to some target state  $\rho^*$  [21] as

$$\mathcal{F}(\rho(t), \rho^*) \equiv \left[ \text{Tr} \left( \sqrt{\sqrt{\rho(t)} \rho^* \sqrt{\rho(t)}} \right) \right]^2. \quad (4)$$

Subsequently, the *error*, or *infidelity*, is then defined as

$$\mathcal{E} \equiv 1 - \mathcal{F}. \quad (5)$$

Since  $\rho^*$  is a pure state ( $\rho^* = |\varphi^*\rangle \langle \varphi^*|$ ) Eq.(4) simplifies to [21]

$$\mathcal{F}(\rho(t), \rho^*) = \text{Tr}(\rho(t) \rho^*). \quad (6)$$

Finally, substituting Eq.(2) into Eq.(6) leads to (see A 1)

$$\mathcal{E}(\rho^*) = \gamma t \Delta_* L + o(\gamma t). \quad (7)$$

where  $\Delta_* L = (\langle L^\dagger L \rangle_* - \langle L^\dagger \rangle_* \langle L \rangle_*)$  with  $\langle L^\dagger L \rangle_* \equiv \text{Tr}(\rho^* L^\dagger L)$ .

### B. Average Gate Fidelity

Only  $\mathcal{E}(\rho^*)$  for a specific  $\rho^*$  was obtained beforehand. However, is there a state-independent approach to obtaining the infidelity of a quantum gate under small-amplitude noise? One defines the quantum gate  $U$  applied during a time duration  $t$ , whose resulting operation brings all initial states  $\rho_0$  to all corresponding  $\rho^* = U \rho_0 U^\dagger$ . There is then a definition of the *average gate fidelity* of a quantum channel  $\mathcal{E}$  attempting to implement the unitary operation  $U$  with a noisy environment which reads as follows [22]

$$\begin{aligned} \bar{\mathcal{F}}(\mathcal{E}, U) &= \int d\rho_0 \mathcal{F}(\rho(t), \rho^*) \\ &= \int d\rho_0 \langle U^\dagger \mathcal{E}[\rho_0] U \rangle_0 = \int d\rho_0 \langle (U^\dagger \circ \mathcal{E}) [\rho_0] \rangle_0, \end{aligned} \quad (8)$$

where the normalized integral is over the Fubini-Study measure on pure states (sometimes called the Haar measure) [23],  $U^\dagger[\rho] \equiv U^\dagger \rho U$  and  $\mathcal{E}[\rho_0] = \rho(t)$ .

Introducing  $\tilde{E}_k = E_k U$  the *Kraus operators* such that

$$\rho(t) = (U^\dagger \circ \mathcal{E}) [\rho_0] = \sum_k \tilde{E}_k \rho_0 \tilde{E}_k^\dagger = \sum_k E_k \rho^* E_k^\dagger, \quad (9)$$

the Average Gate Fidelity  $\bar{\mathcal{F}}$  given in (8) can be rewritten as [24, 25]

$$\bar{\mathcal{F}}(\mathcal{E}, U) = \frac{d + \sum_k |\text{Tr}(\tilde{E}_k U^\dagger)|^2}{d(d+1)} = \frac{d + \sum_k |\text{Tr}(E_k)|^2}{d(d+1)}. \quad (10)$$

Using Eq.(3), one seeks the sets of Kraus operators  $\{\tilde{E}_k\}$  or  $\{E_k\}$  such that

$$\forall \rho_0, \quad \sum_k \tilde{E}_k \rho_0 \tilde{E}_k^\dagger = U \rho_0 U^\dagger - \gamma t \frac{1}{2} \{ L^\dagger L, U \rho_0 U^\dagger \} + \gamma t L U \rho_0 U^\dagger L^\dagger + o(\gamma t) \quad (11a)$$

$$\forall \rho^*, \quad \sum_k E_k \rho^* E_k^\dagger = \rho^* - \gamma t \frac{1}{2} \{ L^\dagger L, \rho^* \} + \gamma t L \rho^* L^\dagger + o(\gamma t). \quad (11b)$$

One can see that the following two sets would work up to the first order in  $\gamma t$

$$\tilde{E}_0 = \left( \mathbb{1}_d - \frac{\gamma t}{2} L^\dagger L \right) U, \quad \tilde{E}_1 = \sqrt{\gamma t} L U, \quad (12a)$$

$$E_0 = \mathbb{1}_d - \frac{\gamma t}{2} L^\dagger L, \quad E_1 = \sqrt{\gamma t} L. \quad (12b)$$

In order to use Eq.(12) in Eq.(8), it is necessary to calculate the traces of the operators. Let us consider a pure dephasing channel i.e.  $\mathcal{E}_z$  with  $L = J_z$  [26]. One obtains a *gate*- (and Hamiltonian-) independent result for the Average Gate Fidelity which reads as (see A 2)

$$\overline{\mathcal{F}}(\mathcal{E}_z) = 1 - \frac{\gamma t}{12} d(d-1) + o(\gamma t). \quad (13)$$

In other words the *Average Gate Infidelity* is given by

$$\overline{\mathcal{E}}(\mathcal{E}_z) = \frac{\gamma t}{12} d(d-1) + o(\gamma t), \quad (14)$$

or more generally for an arbitrary quantum channel  $\mathcal{X}$  with collapse operator  $L$

$$\overline{\mathcal{E}}(\mathcal{X}) = \frac{\gamma t}{d+1} \left( \text{Tr}(L^\dagger L) - \frac{1}{d} |\text{Tr}(L)|^2 \right) + o(\gamma t). \quad (15)$$

Note that it is always possible to find a traceless collapse operator  $L$  emulating  $\mathcal{X}$  [19], so the previous expression can be, in this case, simplified as follows

$$\overline{\mathcal{E}}(\mathcal{X}) = \frac{\gamma t}{d+1} \text{Tr}(L^\dagger L) + o(\gamma t). \quad (16)$$

It follows from (16) that increasing the dimension  $d$  of the Hilbert space would also increase the *robustness* of qudit gates to a dimension-independent quantum channel (if  $L$  is independent of  $d$ ).

### C. Qudits vs. qubits

Now let's apply the same technique as described above to another system: an ensemble of  $n$  identical dephasing qubits (Hilbert space of dimension  $d = 2^n$ ), yielding the master equation

$$\frac{d\rho}{dt} = -i [H, \rho] + \sum_{k=1}^n L_k \rho L_k^\dagger - \frac{1}{2} \sum_{k=1}^n \{ L_k^\dagger L_k, \rho \}, \quad (17)$$

with

$$L_k = \underbrace{\mathbb{1}_2^{(1)} \otimes \cdots \otimes \mathbb{1}_2^{(k-1)}}_{k-1} \otimes S_z^{(k)} \otimes \underbrace{\mathbb{1}_2^{(k+1)} \otimes \cdots \otimes \mathbb{1}_2^{(n)}}_{n-k} \quad (18)$$

for  $k \in \llbracket 1, n \rrbracket$ .

Using the same reasoning as for dephasing qudits one obtains  $n+1$  Kraus operators to first order in  $\gamma t$

$$E_0 = \mathbb{1}_{2^n} - \sum_{k=1}^n \frac{\gamma t}{2} L_k^\dagger L_k, \quad E_k = \sqrt{\gamma t} L_k. \quad (19)$$

In this case (see A 3),

$$\overline{\mathcal{E}}(\mathcal{E}_z) = \frac{\gamma t}{4} \frac{n 2^n}{2^n + 1} + o(\gamma t) = \frac{\gamma t \log_2(d) d}{4(d+1)} + o(\gamma t). \quad (20)$$

Let us stress that (20) yields the same result as Abad *et al.* [27] in the case of identically dephasing qubits with no energy relaxation.

The analytical expressions (16) and (20) are one of the main results of this work.

Following those last two results, two expressions for the AGI have been found: for a single qudit, one finds an infidelity that scales as  $d^2$ :  $\overline{\mathcal{E}}_d(\mathcal{E}_z) = c_d \gamma t$  in (14) and for an ensemble of  $n$  qubits one finds an infidelity that scales as  $\log_2(d)$ :  $\overline{\mathcal{E}}_{b,n}(\mathcal{E}_z) = c_{b,n} \gamma t$  in (20). Moreover, in the case of pure dephasing, one can define the  $T_{2,d}$  dephasing time between two energy-adjacent levels for a qudit. It then shares the same expression (in terms of  $\gamma$ ) as the typical  $T_{2,b}$  dephasing time of a single qubit, namely  $\frac{1}{T_2} = \frac{\gamma}{2}$ .

The ratio between two average gate infidelities, of duration  $t_d$  and  $t_{b,n}$  for qudit and  $n$  qubits, respectively, becomes

$$\frac{\overline{\mathcal{E}}_d(\mathcal{E}_z)}{\overline{\mathcal{E}}_{b,n}(\mathcal{E}_z)} = \frac{c_d t_d / T_{2,d}}{c_{b,n} t_{b,n} / T_{2,b}}. \quad (21)$$

Therefore, in order for a *single* qudit ( $d = 2^n$ ) to outperform *an ensemble* of  $n$  qubits in noise-robustness, i.e., to have a smaller AGI, the following inequality must hold true

$$\frac{t_{b,n} / T_{2,b}}{t_d / T_{2,d}} > \frac{c_d}{c_{b,n}} = \frac{d^2 - 1}{3 \log_2(d)} = \frac{4^n - 1}{3n}. \quad (22)$$

This expression quantifies the requirements on the gate time in decoherence time units  $\tau_d = t_d / T_{2,d}$  relative to  $\tau_{b,n} = t_{b,n} / T_{2,b}$  in order for the qudit to yield higher-fidelity gates. Moreover, it confirms that the infidelity of an ensemble of  $n$  identical qubits and the infidelity of a single qudit will generally not have the same linear behaviour in  $\gamma t$  even if they have the same  $T_2$ , thus simply having  $\tau_d < \tau_{b,n}$  is not sufficient to guarantee a more noise-resilient qudit.

On a side note, the previous calculations could also be applied to an ensemble of  $N$  qudits under identical pure dephasing, in which case we have

$$\overline{\mathcal{E}_{d,N}}(\mathcal{E}_z) = \frac{\gamma t}{12} \frac{Nd^N}{d^N + 1} (d^2 - 1) + o(\gamma t), \quad (23)$$

and for  $2^n = d^N$  one obtains

$$\frac{t_{b,n}/T_{2,b}}{t_{d,N}/T_{2,d}} > \frac{c_{d,N}}{c_{b,n}} = \frac{d^2 - 1}{3 \log_2(d)}. \quad (24)$$

Let us also note that for  $L$  arbitrary (23) yields

$$\overline{\mathcal{E}_{d,N}}(\mathcal{X}) = \gamma t N \frac{d^{N-1}}{d^N + 1} \left( \text{Tr}(L^\dagger L) - \frac{1}{d} |\text{Tr}(L)|^2 \right) + o(\gamma t). \quad (25)$$

#### D. Process fidelity and average of the fluctuation-dissipation relation

One may link the fluctuation-dissipation relation obtained in (7) with the results regarding average gate infidelities from Eq. (15),

$$\overline{\mathcal{E}}(\mathcal{X}) = \gamma t \int d\rho^* \mathcal{E}(\rho^*) = \gamma t \int d\rho^* \Delta_* L + o(\gamma t). \quad (26)$$

This integral over the Fubini-Study measure can formally be computed using Weingarten calculus methods [28] (see A 4) which can be expressed as

$$\int d\rho \Delta L = \frac{1}{d+1} \text{Tr}(L^\dagger L) - \frac{1}{d(d+1)} |\text{Tr}(L)|^2, \quad (27)$$

leading to (15).

In contrast to this formal approach, a more physically-informed approach to obtain the same result was proposed in the previous subsections.

Furthermore, it is possible to express all the computed average gate infidelities as process/entanglement infidelities  $\mathcal{E}^{(p)}$  making use of the relation  $D\overline{\mathcal{E}}^{(p)} = (D+1)\overline{\mathcal{E}}$ , with  $D = d$ ,  $2^n$  or  $d^N$  the dimension of the Hilbert space [29]. This yields the expression

$$\mathcal{E}_{d,n}^{(p)}(\mathcal{X}) = \gamma t \frac{n}{d} \left( \text{Tr}(L^\dagger L) - \frac{1}{d} |\text{Tr}(L)|^2 \right) + o(\gamma t), \quad (28)$$

which is linear in the number of subsystems  $n$ . Likewise we have

$$\mathcal{E}_d^{(p)}(\mathcal{E}_z) = \frac{\gamma t}{12} (d^2 - 1) + o(\gamma t), \quad (29a)$$

$$\mathcal{E}_{b,n}^{(p)}(\mathcal{E}_z) = \frac{\gamma t}{4} n + o(\gamma t). \quad (29b)$$

Note that (29b) has been verified experimentally, for example by Ozaeta and McMahon [30].

### III. SIMULATIONS AND DISCUSSION

All simulations were done using the PYTHON package QUTiP [18] version 4.7, SciPY version 1.7.3, and NUMPy version 1.21.5. For a given dimension, gate, noise parameter and collapse operator, we calculated at different times  $t$ : (i) the propagator superoperators and (ii) the corresponding AGIs. Subsequently, a linear fit for the function  $\overline{\mathcal{E}} = 1 - c\gamma t$  is performed on the AGIs to obtain the gradient  $c$ . In order to obtain a statistically relevant number of gates, many random realizations were generated using a high-performance cluster by computing the corresponding hamiltonians through gradient-ascent methods.

#### A. Fit and deviation from the linear behaviour

This procedure was then applied to single qudits of dimension  $d$  under pure dephasing, with  $H = \mathbb{0}_d$  and small  $\gamma t \in [0, 10^{-6}]$ . The simulations were performed for even dimensions  $d \in [2, 22]$ . Fitting the AGIs  $\overline{\mathcal{E}}_d(\mathcal{E}_z) = c_d \gamma t$  as a function of  $\gamma t$  yielded the slopes  $c_d$  that are shown in Fig.1, along with their analytical expression as a function of  $d$  predicted in (14).

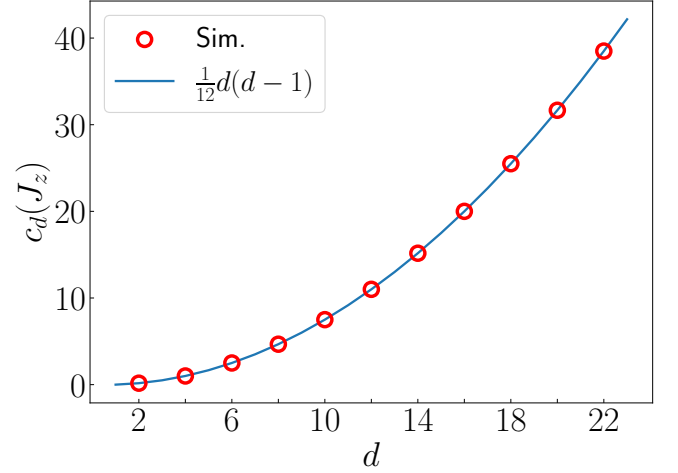


Figure 1. Rate of increase of  $\overline{\mathcal{E}}_d(\mathcal{E}_z) = c_d(J_z)\gamma t$  as a function of qudit dimension for  $H = \mathbb{0}_d$  and  $\gamma t \in [0, 10^{-6}]$ . The circled dots show the numerical results. The solid curve presents the expected analytical result given by (14).

The same simulations were repeated for larger values of  $\gamma t \in [5 \times 10^{-4}, 1 \times 10^{-2}]$  and  $H = \mathbb{0}_d$ . The AGIs were then computed and are shown in Fig.2 alongside the linear infidelity predicted in (14).

For more insight, Fig.3 shows the relative deviation of the computed infidelities from the expected first-order linear behaviour for a broader range of  $\gamma t$  up to  $5 \times 10^{-2}$ .

Average gate infidelities linear in  $\gamma t$  with gradients  $\frac{d(d-1)}{12}$  were expected in the case of a single qudit under pure dephasing, according to (14). Fig.1 supports

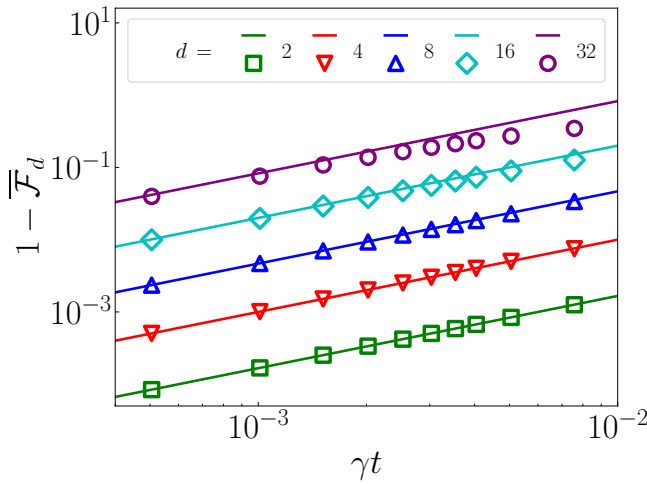


Figure 2. Average gate infidelities as a function of  $\gamma t$ . The data points show the computed values. The solid lines represent the linear theoretical behaviour. Each colour/marker pair corresponds to a different value of  $d$ .

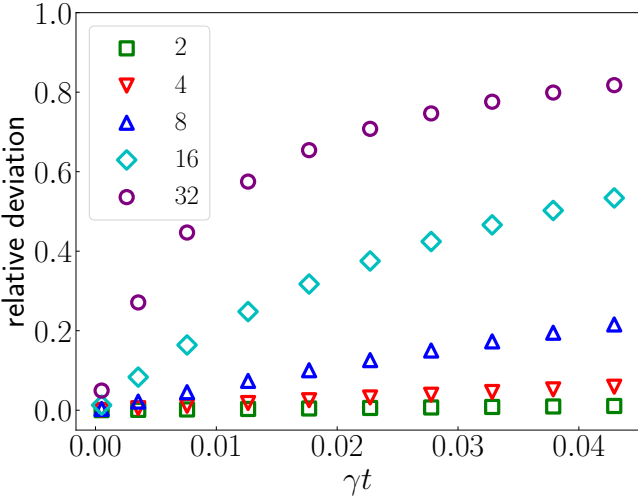


Figure 3. Relative deviation  $1 - \frac{\mathcal{E}_d^{\text{sim}}}{\mathcal{E}_d^{\text{th}}}$  as a function of  $\gamma t$  for  $H = \mathbb{0}_d$ .  $\mathcal{E}_d^{\text{sim}}$  and  $\mathcal{E}_d^{\text{th}}$  were obtained from numerical computations and (14) respectively. Each marker corresponds to a different value of  $d$ .

this for small values of  $\gamma t$ : a least-squares fit of the computed gradients yields the expected relationship with  $1 - R^2 < 10^{-8}$ . Simulations for larger values of  $\gamma t$  (Fig. 2) highlight deviations from this linear behaviour. These originate from  $o(\gamma t)$  terms of the form  $(\gamma t)^{k>1}$  (see Eq. (B8)). Moreover, for fixed values of  $\gamma t$ , as  $d$  increases, the amplitude of this deviation is observed to increase (Fig. 3). This implies that the range of  $\gamma t$  values for which the AGI can be treated linearly diminishes with increasing qudit dimension. Assuming a prefactor of the order  $d^4$  for the  $(\gamma t)^2$  term in the AGI series expansion (as B4 hints), this provides an estimate of the range for which

the deviation from linearity is negligible:  $\gamma t \ll 1$  and  $\frac{1}{d^2}$ .

## B. Gate dependence

While the linearity of the AGI does not scale well with  $d$ , Eq. (14) has another important characteristic that deserves to be studied: the gate independence of the AGI. Unitary quantum gates in  $SU(d)$  were generated randomly and implemented on a qudit through a Hamiltonian obtained by gradient-ascent methods. The AGIs were then computed for  $\gamma t \in [10^{-5}, 10^{-3}]$  and their rate of increase as a function of  $\gamma t$  was fitted. Fig. 4 shows the statistical distributions of the relative deviations from the linear behaviour of the obtained rates.

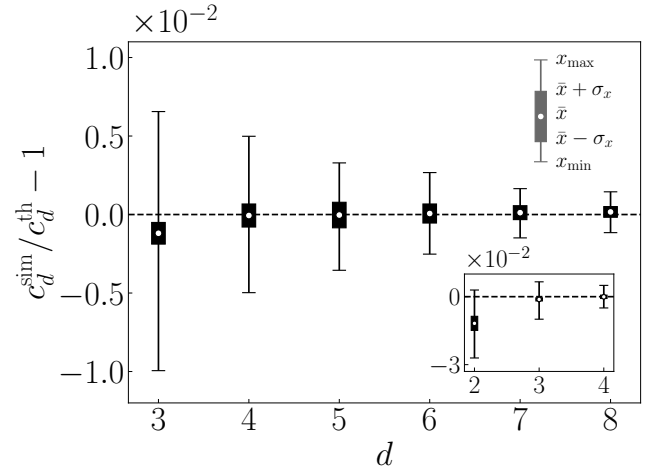


Figure 4. Statistical distributions of the relative deviation from the linear behaviour in (14) of the numerically obtained infidelity gradients  $c_d$  for  $N_g = 5000$  gates for  $\gamma t \in [10^{-5}, 10^{-3}]$ , as a function of the dimension  $d \in [3, 8]$ . The candlestick bar chart should be interpreted as indicated in the upper right. The lower right inset shows the same results for  $d \in [2, 4]$ .

Considering Fig. 4, the relative deviation from the linear behaviour for different random gates seems to exceed 1% rarely and was not observed outside the  $<1\%$  range. Moreover, the range of deviations decreases as the dimension  $d$  increases. The inset highlights a noticeable irregularity for  $d = 2$ , a single qubit, where the relative deviation is of the order of 1%. Note that for the  $H = \mathbb{0}_d$  case simulated in Fig. 1, this shift remained  $<1\%$ , coinciding with the dashed line in Fig. 4, including the case  $d = 2$ . Beginning at  $d = 2$ , the gradient distributions appear broad and off-centred from the  $H = \mathbb{0}_d$  case. As  $d$  increases further, the distributions become progressively concentrated around 0. The gate-dependence also arises from  $o(\gamma t)$  terms, with  $\gamma t^2$  being dominant in the  $\gamma t^2 \|H\| \gtrsim 1$  regime (see Eq. (B7)). Therefore, the AGI can only be considered gate-independent when  $\gamma t \ll 1$  and  $\gamma t \ll \frac{1}{\|H\|t}$ . An informative figure showing the

deviation from linearity and gate-dependence at higher values of  $\gamma t$  is available in Appendix B 1.

### C. Other cases than pure dephasing

Fig.5 shows AGI rates of increase for channels different from pure dephasing namely:  $\overline{\mathcal{E}_d}(\mathcal{E}_x)$ ,  $\overline{\mathcal{E}_d}(\mathcal{E}_+)$ , and  $\overline{\mathcal{E}_d}(\mathcal{E}_{x,y,z})$  corresponding to bit-flip, amplitude damping and depolarizing channels respectively. The simulations were performed again with  $H = \mathbb{0}_d$ , small  $\gamma t \in [0, 10^{-6}]$  and for even dimensions  $d \in [2, 22]$ .

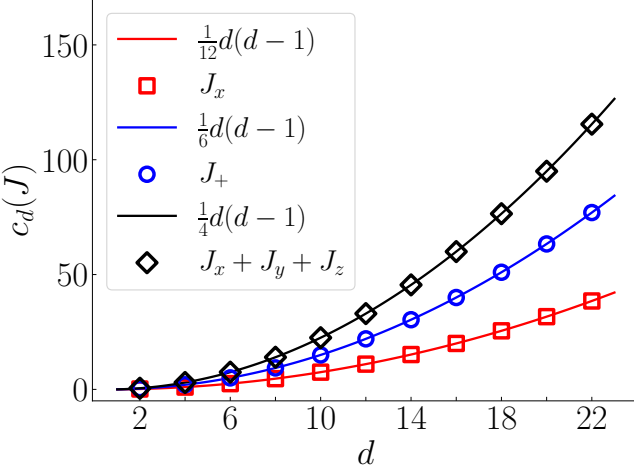


Figure 5. Rate of increase of  $\overline{\mathcal{E}_d}(\mathcal{X}) = c_d(J)\gamma t$  as a function of the qudit dimension with  $H = \mathbb{0}_d$  and  $\gamma t \in [0, 10^{-6}]$ . The markers show the numerical results. The solid curves represent the expected linear responses. Each marker/colour pair corresponds to a different error channel  $\mathcal{X}$ , with collapse operators  $J$  specified in the legend.

Consider  $\mathcal{R}$ , the unitary transformation representing a change of basis, such as a 3D real-space rotation. The average gate fidelity defined in (8) is invariant under the transformation  $\rho \rightarrow \mathcal{R}^\dagger \rho \mathcal{R}$ . This is supported by a comparison of the results for  $L = J_z$  and  $L = J_x$  in Fig.1 and Fig.5, respectively, since the two gradients appear to share the same dependency in  $d$ . Moreover, let  $\{l_k\}$  be an ensemble of traceless collapse operators with corresponding error channels  $\{e_k\}$ , then define  $L = \sum_k l_k$  and associated error channel  $\mathcal{E}$ . From (10) and (12b), as long as  $\text{Tr}(l_k^\dagger l_j) = 0, \forall j \neq k$  then  $\overline{\mathcal{E}}(\mathcal{E}) = \sum_k \overline{\mathcal{E}}(e_k)$ . Fig. 5 again supports such behaviour since simulations with the collapse operator  $L = J_+ \equiv J_x + iJ_y$  yield gradients twice as large as, and  $L = J_x + J_y + J_z$  yield gradients three times as large as, the  $L = J_z$  case.

### D. A single qudit vs an ensemble of qubits

An ensemble of  $n$  qubits were simulated under identical pure dephasing, with  $H = \mathbb{0}_{2^n}$  and small  $\gamma t \in [0, 10^{-6}]$ .

The simulations were performed for  $n \in [1, 7]$ . Fitting the AGI  $\overline{\mathcal{E}_{b,n}(\mathcal{E}_z)} = c_{b,n}\gamma t$  as a function of  $\gamma t$  yielded the slopes  $c_{b,n}$  that are shown in Fig.6, along with their analytical expression as a function of  $d$  given in (20).

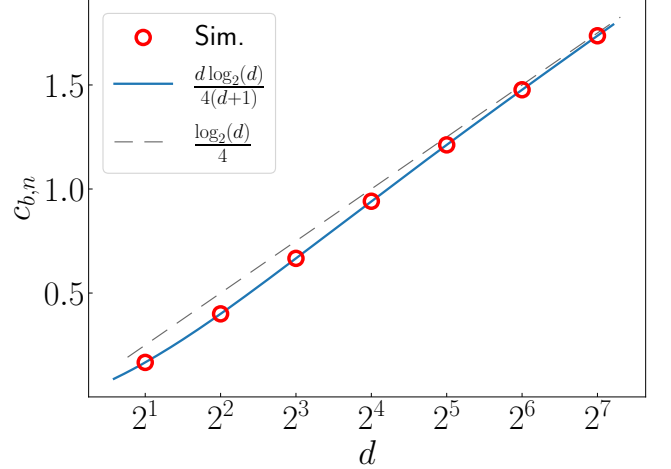


Figure 6. Rate of increase of  $\overline{\mathcal{E}_{b,n}(\mathcal{E}_z)} = c_{b,n}(J_z)\gamma t$  as a function of qudit dimension  $d = 2^n$  with  $H = \mathbb{0}_{2^n}$  and  $\gamma t \in [0, 10^{-6}]$ . The circled dots show the numerical results. The solid curve presents the expected theoretical result. The dashed line shows  $\mathcal{E}_{b,n}^{(p)}(\mathcal{E}_z)$  given in (29b) which is linear in  $n = \log_2(d)$ .

The same simulations were performed on a single qudit with dimension  $d = 2^n$  and Fig.7 shows the ratios  $\frac{c_d}{c_{b,n}}$  for  $n \in [1, 6]$  as well as the theoretical curve provided by Eq. (22) on which the points should be falling. According to the same Eq. (22), this curve also highlights the critical values of  $\tau_b/\tau_d$ , denoting  $\tau_k = t_k/T_{2,k} = \gamma_k t_k/2$ , with respect to qudit/qubits advantage in terms of the rate of increase of the AGI.

The AGI gradients obtained for an ensemble of  $n$  qubits under identical pure dephasing were expected to follow a  $\frac{d \log_2(d)}{4(d+1)}$  relationship as a function of  $d$  (20). Fig.6 justifies this for small values of  $\gamma t$  with the least-square fit now yielding  $1 - R^2 < 10^{-10}$ . Finally, Fig. 7 provides quantitative data for the ratio of the decoherence times of a single qudit vs an ensemble of qubits. Some values of interest are summarised in Table I. For example, in order for a qu8it ( $d = 8$ ) to present a computational fidelity advantage over 3 qubits for a fixed gate time, the qudit platform needs a coherence time at least 7 times longer than the multiqubit platform.

From Table II, state-of-the-art single qudit platforms, such as trapped ions [3], present coherence times of the order of 100ms for a single qu7it, orders of magnitude longer than superconducting qubits [30, 36–38]. Trapped ions present  $\gamma t \approx 10^{-3}$ , while  $\gamma t \approx 10^{-2}$  for superconducting qubits; this ratio of 10 would allow qudits with  $d \lesssim 10$  to still be advantageous. Another comparison with superconducting qubits could be molecular qudits, where some proposals put  $\gamma t \approx 10^{-4}$  [1], and whose co-

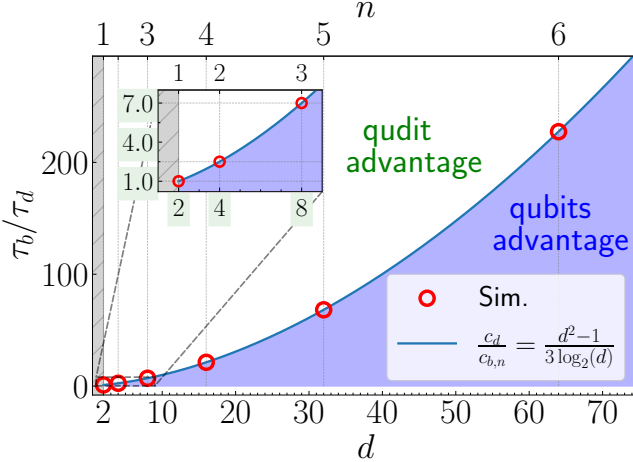


Figure 7. Potential range for  $\tau_b/\tau_d$ . The rounded circles show the numerical values obtained for  $c_d/c_{b,n}$ . The solid curve comes from (22) and highlights the theoretical critical values of  $T_{2,d}/T_{2,b}$ .

Number $n$ of qubits	1	2	3	6
Dimension $d$ of the qudit	2	4	8	64
Critical $\tau_b/\tau_d$	1	2.5	7	227.5

Table I. Ratios of gate times in units of decoherence times between qubits and qudits for specific values of  $n$  and  $d$ .  $\tau_b/\tau_d$  needs to be larger than the critical values in order for a single qudit to be advantageous vs an equivalent ensemble of  $n$  qubits.

herence times are  $\sim 6 - 7$  times larger than the superconducting qubit case. In the latter, with a  $\tau$  ratio of  $\sim 100$ , single qudits with  $d \lesssim 40$  are still advantageous over equivalent superconducting qubits, i.e.  $n \sim 5$ . Such high- $d$  qudit platforms can still be conceivable, given that some specific quantum operations on  $d = 52$  have already successfully been implemented on Rydberg atoms [35], for example.

Finally, one can compare (22) and (24) to discuss conditions on  $N$  qudits outperforming  $N \log_2(d)$  qubits. From this, if a single qudit outperforms  $\log_2(d)$  qubits, the advantage remains conserved as long as the multi-qudit gate time scales slower from 1 qudit to  $N$  qudits than the multiqubit from  $\log_2(d)$  to  $N \log_2(d)$  qubits.

#### IV. CONCLUSION

Given the rapid development of quantum computing platforms with very different physical properties, such as decoherence time or Hilbert space dimension (see Table II), there is a growing need for detailed elaboration of the tradeoffs between their information density and

	$d$	$n$	$T_2$	$t_n$	$\tau_n$	ref.
qubits	2	2	$\sim 10$ $\mu$ s	60 ns	$\sim 10^{-2}$	[31] (2020)
	2	2	$\sim 2$ $\mu$ s	51 ns	$\sim 10^{-2}$	[32] (2020)
	2	17	$\sim 30$ $\mu$ s	$\sim 100$ ns	$\sim 10^{-3}$	[33] (2022)
	2	24	$\sim 100$ ms	$\sim 200$ $\mu$ s	$\sim 10^{-3}$	[34] (2021)
qudits	4	1	0.32 ms	$\sim 100$ ns	$\sim 10^{-4}$	[1] (2018)
	3	2	$\sim 100$ ms	$\sim 100$ $\mu$ s	$\sim 10^{-3}$	[3] (2022)
	4	2	$\infty^a$	—	0	[2] (2022)
	52	1	—	$\sim 100$ ns <sup>b</sup>	—	[35] (2020)

superconducting qubits, Rydberg atoms, trapped ions

molecular nuclear spins, photonic qudits

<sup>a</sup> considered unlimited by the source authors

<sup>b</sup> no universal gates for the moment, only specific quantum operations implemented

Table II. Decoherence times ( $T_2$ ) and gate times ( $t_n$ ) of different qubit/qudit platforms.  $d$  and  $n$  are the maximum dimension and number of qudits an operation was applied to, while  $\tau_n = t_n/T_2$ .

noise error rates. By combining analytical results and numerical simulations, we have performed a comparative study of gate efficiency for systems composed of sets of qubits or qudits. A fluctuation-dissipation-like relation for the gate infidelity of an operation on a pure state was derived. We then put forward a physically-informed method to obtain the first-order effect of Markovian noise on the *average gate infidelity* (AGI). A connection was made between the latter and the first gate-independent result. The rate of increase of the AGI of a single qudit vs equivalent multiple qubits under pure dephasing was compared. This yielded a critical curve of the ratio of their respective gate times in units of decoherence time, a quantity indicating how time-efficient operations on a particular system are. Values on either side of the curve specify which of the two systems had a higher rate of increase of the AGI. To compete in terms of gate fidelity, as the dimension increases, the efficiency of qudit gates must always be larger than the multiqubit one by a factor  $O(d^2/\log_2(d))$ . Additionally, analytical expressions of linear response for arbitrary collapse operators and a general multiqudit system were presented (see (16) and (25)). They may be useful to those working in the field of quantum computing.

Numerical simulations contributed to the discussion on the validity and limits of the linear response assumption. This further restricted the ranges of possible  $\gamma t \ll 1$  accounting for qudit dimension, gate, and noise type. For example, the larger the dimension, the lower the relative gate-dependent response. Finally, after simulations

supported the analytical critical curve, different current platforms were studied with respect to this condition on gate time efficiency. Given equivalent Hilbert space dimensions, viable qudit platforms capable of outperforming equivalent state-of-the-art multiqubit ones in gate fidelity have been found for pure dephasing. Moreover, this performance could be extended to qudits with  $d$  as large as  $\sim 40$  in the case of nuclear molecular magnets, for example. Some multiqubit platforms still outperform any existing qudit platform regarding scalability in the number of subsystems. However, it is conceivable that some scalable qudit platforms continue to outperform equivalent multiqubit systems in terms of attainable fidelity. Further study of how multiqudit and multiqubit gate times scale with the number of subsystems is needed. Moreover, this study was limited to first-order noise responses. However, some quantum error correction schemes recently demonstrated it is possible to entirely remove the first-order response of logical qukits embedded in physical qudits ( $k < d$ ) through carefully chosen encodings [9, 10]. An additional study of higher-order responses of logical qudits vs. physical qubits would therefore also be required to assess the viability of these logical error-resilient qudits. This could elucidate if qudit advantage is robust to system scaling and if qudits will remain useful beyond the NISQ era.

## ACKNOWLEDGMENTS

This work was funded by the French National Research Agency (ANR) through the Programme d’Investissement d’Avenir under contract ANR-11-LABX-0058\_NIE and ANR-17-EURE-0024 within the Investissement d’Avenir program ANR-10-IDEX-0002-02. J-G.H. also acknowledges QUSTEC funding from the European Union’s Horizon 2020 research and innovation program under the Marie Skłodowska-Curie Grant Agreement No. 847471. The authors would like to acknowledge the High Performance Computing Center of the University of Strasbourg for supporting this work by providing scientific support and access to computing resources. Part of the computing resources were funded by the Equipex Equip@Meso project (Programme Investissements d’Avenir) and the CPER Alsacalcul/Big Data.

## Appendix A: Complementary Derivations

### 1. Fluctuation-dissipation relation

Substituting Eq.(3) and Eq.(2) into Eq.(6) and Eq.(5) leads to

$$\mathcal{E}(\rho^*) = \gamma t \left( \frac{1}{2} \text{Tr}(\rho^* \{L^\dagger L, \rho^*\}) - \text{Tr}(\rho^* L \rho^* L^\dagger) \right) + o(\gamma t). \quad (\text{A1})$$

The trace being invariant by cyclic permutations and  $\rho^{*2} = \rho^*$  leads to the simplification

$$\frac{1}{2} \text{Tr}(\rho^* \{L^\dagger L, \rho^*\}) = \text{Tr}(\rho^* L^\dagger L) \equiv \langle L^\dagger L \rangle_* . \quad (\text{A2})$$

Moreover

$$\text{Tr}(\rho^* L \rho^* L^\dagger) = \text{Tr}(|\varphi^*\rangle \langle \varphi^*| L |\varphi^*\rangle \langle \varphi^*| L^\dagger) \quad (\text{A3})$$

$$= \langle L \rangle_* \text{Tr}(\rho^* L^\dagger) \quad (\text{A4})$$

$$= \langle L^\dagger \rangle_* \langle L \rangle_* . \quad (\text{A5})$$

Accounting for the above results, one finally obtains

$$\mathcal{E}(\rho^*) = \gamma t (\langle L^\dagger L \rangle_* - \langle L^\dagger \rangle_* \langle L \rangle_*) + o(\gamma t), \quad (\text{A6})$$

which can be rewritten as Eq. (7).

### 2. Average Gate Infidelity for the Pure Dephasing Channel of one qudit

In a trivial way we have  $\text{Tr}(E_1) \propto \text{Tr}(J_z) = 0$ , and

$$\begin{aligned} \text{Tr}(E_0) &= d - \frac{\gamma t}{2} \text{Tr}(J_z^2) \\ &= d - \frac{\gamma t}{2} \sum_{k=0}^{d-1} \left( \frac{d-1-2k}{2} \right)^2 \\ &= d - \frac{\gamma t}{8} \left[ d(d-1)^2 - 4(d-1) \sum_{k=0}^{d-1} k + 4 \sum_{k=0}^{d-1} k^2 \right] \\ &= d - \frac{\gamma t}{8} \left[ d(d-1)^2 - 2d(d-1)^2 + 4 \frac{d(d-1)(2d-1)}{6} \right] \\ &= d - \frac{\gamma t}{24} d(d^2 - 1), \end{aligned}$$

which results in

$$|\text{Tr}(E_0)|^2 = d^2 - \frac{\gamma t}{12} d^2(d^2 - 1) + o(\gamma t) . \quad (\text{A7})$$

Therefore

$$\overline{\mathcal{E}}(\mathcal{E}_z) = \frac{d + d^2 - \frac{\gamma t}{12} d^2(d^2 - 1)}{d(d+1)} + o(\gamma t) , \quad (\text{A8})$$

which leads to the simplified expression (13).

### 3. Average Gate Infidelity for the pure dephasing channel of $n$ qubits

Since  $\text{Tr}(E_k) = 0 \ \forall k \neq 0$ , only  $\text{Tr}(E_0)$  is left and is given by

$$\begin{aligned} \text{Tr}(E_0) &= 2^n - \frac{\gamma t}{2} \sum_{k=1}^n \left[ \text{Tr}(S_z^{2(k)}) \prod_{j \neq k} \text{Tr}(\mathbb{1}_2^{2(j)}) \right] \\ &= 2^n - n \frac{\gamma t}{8} 2^n, \end{aligned} \quad (\text{A9})$$

leading to

$$|\text{Tr}(E_0)|^2 = 2^{2n} - \frac{\gamma t}{4} n 2^{2n} + o(\gamma t), \quad (\text{A10})$$

which allows to obtain (20) using (10).

#### 4. Average over the Fubini-Study measure of the uncertainty of $L$

First, rewriting  $\int d\rho \text{Tr}(\rho M^\dagger M)$  yields

$$\int dU \text{Tr}(U\rho U^\dagger M^\dagger M) = \text{Tr} \left[ \left( \int dU U\rho U^\dagger \right) M^\dagger M \right]$$

, where the integration is performed over the uniform Haar measure in the space of unitaries. Using the identity

$$\int dU UXU^\dagger = \frac{\text{Tr}(X)I}{d}$$

valid for any linear operator  $X$ , for the special case of  $\rho$  pure one obtains

$$\int d\rho \text{Tr}(\rho M^\dagger M) = \frac{1}{d} \text{Tr}(M^\dagger M). \quad (\text{A11})$$

Now, rewriting  $\int d\rho \text{Tr}(\rho M^\dagger M)$  yields

$$\begin{aligned} & \int dU \text{Tr}(U\rho U^\dagger M)^2 = \\ & \sum_{i,j,k,l} \int dU U_{ij} U_{k\ell} \bar{U}_{mn} \bar{U}_{pq} \rho_{jn} \rho_{\ell q} M_{mi} M_{pk}. \end{aligned}$$

Collins *et al.* [28] provides formulae to integrate polynomials of unitary matrices

$$\begin{aligned} & \int_{U_d} dU U_{ij} U_{k\ell} \bar{U}_{mn} \bar{U}_{pq} = \\ & \frac{1}{d^2 - 1} \left[ (\delta_{im} \delta_{jn} \delta_{kp} \delta_{\ell q} + \delta_{ip} \delta_{jq} \delta_{km} \delta_{\ell n}) \right. \\ & \left. - \frac{1}{d} (\delta_{im} \delta_{jq} \delta_{kp} \delta_{\ell n} + \delta_{ip} \delta_{jn} \delta_{km} \delta_{\ell q}) \right], \quad (\text{A12}) \end{aligned}$$

which contracting the indices gives

$$\int d\rho |\text{Tr}(\rho M)|^2 = \frac{1}{d(d+1)} (\text{Tr}(M^\dagger M) + |\text{Tr}(M)|^2).$$

Finally subtracting (A12) from (A11) leads to (27).

#### Appendix B: Higher-order effects of the collapse operators

##### 1. Complementary figure : deviation from linearity and gate dependence

Fig.8 allows for observation of (i) the deviation from linear behaviour as  $\gamma t$  increases, (ii) for higher  $d$ , this deviation becomes noticeable for smaller values of  $\gamma t$  and, (iii) the infidelity becomes increasingly gate-dependent as  $\gamma t$  increases.

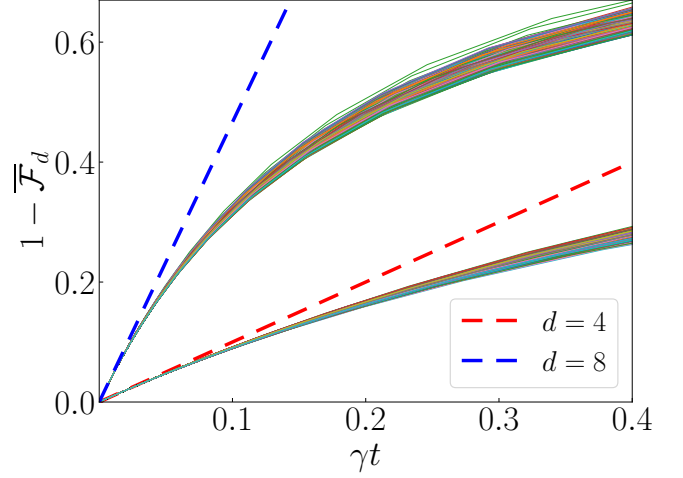


Figure 8. Simulated AGIs of  $N_g = 4400$  gates for  $d = 4, 8$  in solid lines. The dashed lines correspond to the expected linear behaviour at small  $\gamma t$ .

#### 2. Full expansion of the density matrix

The density matrix  $\rho(t)$  can be decomposed as

$$\rho(t) = \rho^* + \sum_{l=1} \sum_{k=1} \rho_{lk} \gamma^l t^k. \quad (\text{B1})$$

Substituting Eq. (B1) in (1) yields the following results:

- $\rho_{11} = \mathcal{D}[\rho^*] := \sum_k L_k \rho^* L_k^\dagger - \frac{1}{2} \{ L_k^\dagger L_k, \rho^* \}$  .
- for  $l \geq 2$ ,  $k = 1$ ,  $\rho_{l,1} = 0$  .
- for  $l = 1$ ,  $k \geq 2$ ,

$$k \rho_{1k} = -i[H, \rho_{1(k-1)}] - \dot{\rho}_{1(k-1)}. \quad (\text{B2})$$

- $\forall l, k \geq 2$ ,

$$k \rho_{lk} = -i[H, \rho_{l(k-1)}] - \dot{\rho}_{l(k-1)} + \mathcal{D}[\rho_{(l-1)(k-1)}]. \quad (\text{B3})$$

It can be linked to (3) by noticing that  $M = -\rho_{11}$ .

Moreover, for  $k = l = 2$  we obtain

$$\rho_{22} = \mathcal{D}[\rho_{11}] = \mathcal{D}[\mathcal{D}[\rho^*]]. \quad (\text{B4})$$

Finally we have

$$\rho_{12} = \frac{i}{2} (\mathcal{D}[[H, \rho^*]] - [H, \rho^*]), \quad (\text{B5})$$

and

$$\rho_{13} = -\frac{i}{3} [H, \rho_{12}] - \frac{\dot{\rho}_{12}}{3}. \quad (\text{B6})$$

This gives us the following expansion

$$\rho(t) = \rho^* + \gamma t \rho_{11} + \gamma t^2 \rho_{12} + \gamma t^3 \rho_{13} + (\gamma t)^2 \rho_{22} + \epsilon, \quad (\text{B7})$$

with  $\epsilon = O(\gamma^l t^k)_{l+k \geq 5}$ .

Interestingly, it can be proven by induction that if  $H = \mathbb{0}_d$  then,

$$\rho(t) = \rho^* + \sum_k (\gamma t)^k \rho_{kk}, \quad (\text{B8})$$

[1] E. Moreno-Pineda, C. Godfrin, F. Balestro, W. Wernsdorfer, and M. Ruben, *Chemical Society Reviews* **47**, 501 (2018).

[2] Y. Chi, J. Huang, Z. Zhang, J. Mao, Z. Zhou, X. Chen, C. Zhai, J. Bao, T. Dai, H. Yuan, *et al.*, *Nature Communications* **13**, 1166 (2022).

[3] M. Ringbauer, M. Meth, L. Postler, R. Stricker, R. Blatt, P. Schindler, and T. Monz, *Nature Physics* **18**, 1053 (2022).

[4] N. P. Brusentsov and J. Ramil Alvarez, in *Perspectives on Soviet and Russian Computing*, IFIP Advances in Information and Communication Technology, edited by J. Impagliazzo and E. Proydakov (Springer, Berlin, Heidelberg, 2011) pp. 74–80.

[5] S. Boixo, S. V. Isakov, V. N. Smelyanskiy, R. Babbush, N. Ding, Z. Jiang, M. J. Bremner, J. M. Martinis, and H. Neven, *Nature Physics* **14**, 595 (2018).

[6] F. Arute, K. Arya, R. Babbush, D. Bacon, J. C. Bardin, R. Barends, R. Biswas, S. Boixo, F. G. S. L. Brandao, D. A. Buell, *et al.*, *Nature* **574**, 505 (2019).

[7] IBM Unveils 400 Qubit-Plus Quantum Processor and Next-Generation IBM Quantum System Two (2022).

[8] Y. Wang, Z. Hu, B. C. Sanders, and S. Kais, *Frontiers in Physics* **8** (2020).

[9] A. Chiesa, F. Petiziol, E. Macaluso, S. Wimberger, P. Santini, and S. Carretta, *AIP Advances* **11**, 025134 (2021).

[10] F. Petiziol, A. Chiesa, S. Wimberger, P. Santini, and S. Carretta, *npj Quantum Information* **7**, 1 (2021).

[11] W. Wernsdorfer and M. Ruben, *Advanced Materials* **31**, 1806687 (2019).

[12] Y. Zheng, H. Sharma, and J. Borregaard, *PRX Quantum* **3**, 040319 (2022).

[13] F. Bouchard, R. Fickler, R. W. Boyd, and E. Karimi, *Science Advances* **3**, e1601915 (2017).

[14] E. T. Campbell, H. Anwar, and D. E. Browne, *Physical Review X* **2**, 041021 (2012).

[15] C. Godfrin, A. Ferhat, R. Ballou, S. Klyatskaya, M. Ruben, W. Wernsdorfer, and F. Balestro, *Physical Review Letters* **119**, 187702 (2017).

[16] S. Thiele, F. Balestro, R. Ballou, S. Klyatskaya, M. Ruben, and W. Wernsdorfer, *Science* **344**, 1135 (2014).

[17] M. Otten, K. Kapoor, A. B. Özgüler, E. T. Holland, J. B. Kowalkowski, Y. Alexeev, and A. L. Lyon, *Physical Review A* **104**, 012605 (2021).

[18] J. Johansson, P. Nation, and F. Nori, *Computer Physics Communications* **183**, 1760 (2012).

[19] D. Manzano, *AIP Advances* **10**, 025106 (2020).

[20] We define here that  $g(\gamma, t) = o(\gamma t) \Leftrightarrow g(\gamma, t)/(\gamma t) \rightarrow 0$  as  $\gamma$  and  $t \rightarrow 0$ . It comprises here terms of the form  $(\gamma^l t^k)_{l+k \geq 3}$ , a more in-depth discussion is available in

with  $\rho_{kk} = \frac{1}{k!} \mathcal{D}^{(k)}[\rho^*]$ .

## Appendix B.

[21] R. Jozsa, *Journal of Modern Optics* **41**, 2315 (1994).

[22] M. A. Nielsen, *Physics Letters A* **303**, 249 (2002).

[23] J. Qi and H. K. Ng, *International Journal of Quantum Information* **17**, 1950031 (2019).

[24] N. Johnston and D. W. Kribs, *Journal of Physics A: Mathematical and Theoretical* **44**, 495303 (2011).

[25] E. Magesan, *Gaining Information About a Quantum Channel Via Twirling*, Master's thesis, University of Waterloo (2008).

[26] W. Zhong, Z. Sun, J. Ma, X. Wang, and F. Nori, *Physical Review A* **87**, 022337 (2013).

[27] T. Abad, J. Fernández-Pendás, A. Frisk Kockum, and G. Johansson, *Physical Review Letters* **129**, 150504 (2022).

[28] B. Collins, S. Matsumoto, and J. Novak 10.48550/ARXIV.2109.14890 (2021).

[29] M. Horodecki, P. Horodecki, and R. Horodecki, *Physical Review A* **60**, 1888 (1999).

[30] A. Ozaeta and P. L. McMahon, *Quantum Science and Technology* **4**, 025015 (2019).

[31] M. Kjaergaard, M. E. Schwartz, A. Greene, G. O. Samach, A. Bengtsson, M. O'Keeffe, C. M. McNally, J. Braumüller, D. K. Kim, P. Krantz, *et al.* 10.48550/ARXIV.2001.08838 (2020).

[32] I. S. Madjarov, J. P. Covey, A. L. Shaw, J. Choi, A. Kale, A. Cooper, H. Pichler, V. Schkolnik, J. R. Williams, and M. Endres, *Nature Physics* **16**, 857 (2020).

[33] S. Krinner, N. Lacroix, A. Remm, A. Di Paolo, E. Genois, C. Leroux, C. Hellings, S. Lazar, F. Swiadek, J. Herrmann, G. J. Norris, C. K. Andersen, M. Müller, A. Blais, C. Eichler, and A. Wallraff, *Nature* **605**, 669 (2022).

[34] I. Pogorelov, T. Feldker, C. D. Marciak, L. Postler, G. Jacob, O. Kriegsteiner, V. Podlesnic, M. Meth, V. Negnevitsky, M. Stadler, B. Höfer, C. Wächter, K. Lakhmanskii, R. Blatt, P. Schindler, and T. Monz, *PRX Quantum* **2**, 020343 (2021).

[35] A. Larrouy, S. Patsch, R. Richaud, J.-M. Raimond, M. Brune, C. P. Koch, and S. Gleyzes, *Physical Review X* **10**, 021058 (2020).

[36] Y. Chen, C. Neill, P. Roushan, N. Leung, M. Fang, R. Barends, J. Kelly, B. Campbell, Z. Chen, B. Chiaro, *et al.*, *Physical Review Letters* **113**, 220502 (2014).

[37] M. Kjaergaard, M. E. Schwartz, J. Braumüller, P. Krantz, J. I.-J. Wang, S. Gustavsson, and W. D. Oliver, *Annual Review of Condensed Matter Physics* **11**, 369 (2020).

[38] S. Rosenblum, Y. Y. Gao, P. Reinhold, C. Wang, C. J. Axline, L. Frunzio, S. M. Girvin, L. Jiang, M. Mirrahimi, M. H. Devoret, and R. J. Schoelkopf, *Nature Communications* **9**, 652 (2018).